

THE ROLE OF BODY FLEXIBILITY IN STROKE ENHANCEMENTS FOR FINITE-LENGTH UNDULATORY SWIMMERS IN VISCOELASTIC FLUIDS

BECCA THOMASES AND ROBERT D. GUY

ABSTRACT. The role of passive body dynamics on the kinematics of swimming micro-organisms in complex fluids is investigated. Asymptotic analysis of small amplitude motions of a finite-length undulatory swimmer in a Stokes-Oldroyd-B fluid is used to predict shape changes that result as body elasticity and fluid elasticity are varied. Results from the analysis are compared with numerical simulations, and the small amplitude analysis of shape changes is quantitatively accurate at both small and large amplitudes, even for strongly elastic flows. We compute a stroke-induced swimming speed that accounts for the shape changes, but not additional effects of fluid elasticity. Elastic induced shape changes lead to larger amplitude strokes for sufficiently soft swimmers in a viscoelastic fluid, and these stroke boosts can lead to swimming speed-ups, but we find that additional effects of fluid elasticity generically slow down swimmers. High amplitude strokes in strongly elastic flows lead to a qualitatively different regime in which highly concentrated elastic stresses accumulate near swimmer bodies and where dramatic slow-downs are seen.

1. INTRODUCTION

There has been an intense effort over the past 10 years to understand the effect of fluid elasticity on micro-organism swimming. Experiments, analysis, and simulations of low-Reynolds number swimming of microorganisms in complex fluids, in particular viscoelastic fluids, has led to a variety of results – some complimentary, some apparently conflicting – on the effect of fluid elasticity on swimming speed. We know that gait, body stiffness, and nonlinear effects matter, but we still do not have a clear understanding of how they interact during locomotion.

Here we focus on undulatory swimmers in an Oldroyd-B fluid. A key question is: Can fluid elasticity enhance swimming speed? Asymptotic analysis of infinitely long, small-amplitude swimmers has shown that swimming is hindered by the addition of elastic stresses [1], although allowing for flexibility can lead to enhancements [2]. Biological experiments have shown a viscoelastic slow-down for *C. elegans* [3], while simulations of finite-length swimmers with large tail amplitudes [4, 5] give a non-monotonic boost as fluid elasticity is varied. In [5] we concluded that shape changes due to body flexibility and fluid elasticity are important, but those results did not explain the results from a physical experiment which showed monotonic speed-ups due to fluid elasticity in swimmers with large tail amplitudes [6]. Furthermore, recent numerical simulations [7] appear to contradict the speed-ups reported in [4, 5].

There remains a gap between our understanding from analysis and what we see in computational, biological, and physical experiments. Here we combine analysis with numerical simulations of finite-length large amplitude swimmers to show how fluid elasticity induces shape changes in flexible swimmers and how those shape changes can lead to speed boosts. We show how shape changes depend on both body stiffness as well as fluid elasticity and analyse the effect that shape changes have on swimming speed.

2. EFFECT OF PASSIVE BODY DYNAMICS

2.1. Methodology. We follow the computational framework in [5, 8], where the swimmer is modeled as an inextensible flexible sheet of finite-length L immersed in a 2D fluid. We describe the undulatory motion of the swimmer by a curvature of the form

$$(1) \quad \kappa_0(s, t) = (A_t(L - s)/L + A_h s/L) \sin(2\pi t/T + \pi s),$$

where $s \in [0, L]$ is the body coordinate. Here A_t is the curvature amplitude at the “tail” ($s = 0$) and A_h is the curvature amplitude at the “head” ($s = L$) of the swimmer.

We use the immersed boundary method to solve for the coupled motion of the fluid and the swimmer [9]. Both inextensibility and shape are imposed (approximately) by forces that are designed to penalize extension and deviation from the prescribed target curvature. These forces are derived from the variation of bending and extension (stretching) energy functionals. For example, the bending energy is $E_b = B/2 \int_{\Gamma} (\kappa - \kappa_0)^2 ds$, where B is the bending stiffness, κ is the curvature of the sheet, and κ_0 is the prescribed target curvature. One can interpret the model as an active sheet with bending stiffness B driven by an active body moment density $B\kappa_0$. We scale forces relative to viscous forces so that for $B \gg 1$, the realized shape of the swimmer is very close to the prescribed shape. For $B \sim 1$, the realized shape is the result of fluid-structure interaction; i.e. passive body dynamics influence the resulting stroke.

The viscoelastic fluid is described by the Oldroyd-B model at zero Reynolds number [10], regularized by stress diffusion [11, 12]. The system of equations describing the fluid are

$$(2) \quad \Delta \mathbf{u} - \nabla p + \xi \nabla \cdot \boldsymbol{\tau}_p + \mathbf{f} = 0, \text{ and } \nabla \cdot \mathbf{u} = 0,$$

$$(3) \quad \text{De}(\partial \boldsymbol{\tau}_p / \partial t + \mathbf{u} \cdot \nabla \boldsymbol{\tau}_p - \nabla \mathbf{u} \boldsymbol{\tau}_p - \boldsymbol{\tau}_p \nabla \mathbf{u}^T) + \boldsymbol{\tau}_p = \dot{\boldsymbol{\gamma}} + \text{De} \varepsilon \Delta \boldsymbol{\tau}_p$$

where \mathbf{u} is the fluid velocity, p is the pressure, $\boldsymbol{\tau}_p$ is the viscoelastic stress, $\dot{\boldsymbol{\gamma}}$ is the rate of strain tensor, and \mathbf{f} is the elastic force density generated by the swimmer. Here ξ is the polymer to solvent viscosity ratio, $\text{De} = \lambda/T$, the Deborah number is the ratio of elastic relaxation time to stroke period, and $\varepsilon \ll 1$ is the stress diffusion coefficient.

The system is solved in a 2D periodic domain of size $[0, 2] \times [0, 2]$, with $L = 1$, $dt = 10^{-3}$, and $dx = 2^{-8}$. We fix $\xi = 0.5$, consistent with [4], and $\varepsilon = 0.0015$ which provides a regularization to control large stress gradient growth [12]. We enforce inextensibility with a dimensionless stiffness constant of 2500.

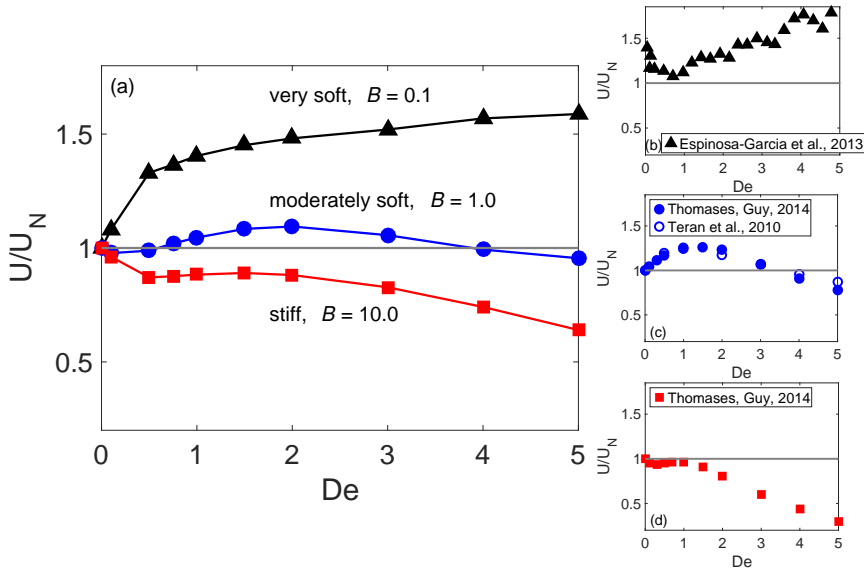


FIGURE 1. Normalized swimming speed as a function of De for different bending stiffness B , with $T = 1$. The right column has reproductions of data from literature.

2.2. Varying body stiffness. To understand the role of body elasticity, we use our simulations to calculate the Stokes-normalized swimming speed while varying B and De for a fixed period ($T = 1$). We use a stroke defined by equation (1) with $A_t = 5$, and $A_h = 2$. This gives a high-amplitude stroke like in [4, 5]. In figure 1(a) we plot normalized swimming speed as a function of De for three characteristic stiffness values of $B = 0.1, 1.0, 10.0$, which we refer to as *very soft*, *moderately soft*, and *stiff*, respectively. For *very soft* swimmers we see a monotonic boost in swimming speed, with a greater than 50% boost for high De . This response is similar to what was reported in [6] using a physical model of a swimmer with a flexible tail (figure 1(b)). For *moderately soft* swimmers, we see a non-monotonic speed-up, including a smaller speed boost over the Newtonian speed, followed by a slow-down at larger De . This type of non-monotonic speed-up was first reported in [4] and again in [5] for a soft stroke with high amplitude (figure 1(c)). Finally, for *stiff* swimmers we see non-monotonic behavior but no boost over the Newtonian speed, again followed by a slow-down at larger De . This type of slow-down was reported in [5] for a stiff kicker (figure 1(d)).

In contrast to stiff, or rigid, swimmers, the dynamics of flexible swimmers involve an additional time scale. In a viscous fluid, rigid swimmers move with a velocity proportional to the beat frequency (the only time scale in the problem). The problem of a rigid swimmer in a viscoelastic fluid has two time scales, the beat frequency and the relaxation time, whose ratio is the dimensionless relaxation time De . The swimming speed of soft swimmers depends nonlinearly on the frequency because the shape changes with the frequency. To

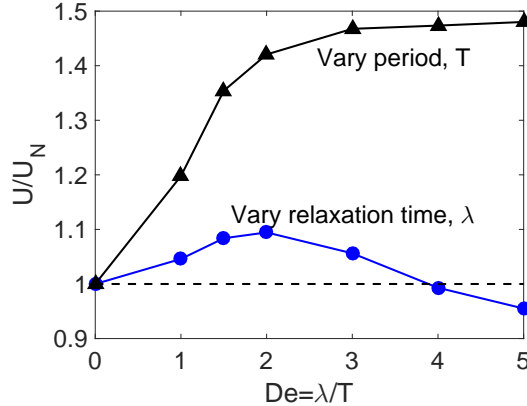


FIGURE 2. Normalized swimming speed as a function of De . Curves generated by varying only relaxation time (for fixed period $T = 1$) or stroke period (for fixed relaxation time $\lambda = 0.5$). Body stiffness is fixed: $B = 1.0$.

illustrate the significance of multiple time scales for flexible swimmers in viscoelastic fluids we compute the Stokes-normalized swimming speed as a function of De varied two ways: by varying the relaxation time for a fixed period, and by varying the period for a fixed relaxation time. Both simulations are performed with the same bending stiffness, $B = 1.0$, where passive body dynamics are significant. Results are shown in figure 2 for a swimmer with the same stroke from figure 1, and the two curves show remarkable qualitative differences. For a rigid swimmer these would give equivalent results. Thus this third time-scale, arising from body flexibility, needs to be explicitly included in any discussion of swimming in elastic fluids.

3. ANALYSIS OF SHAPE CHANGES

The effect of body stiffness on swimming kinematics has been previously studied for viscous fluids [13, 14]. Shape changes in viscoelastic fluids have been examined [15], but the relationship between shape changes and swimming speed has not been examined for finite-length swimmers. Here we review the theory and compare it with numerical simulations.

3.1. Linear theory: viscous fluids. We begin by considering small amplitude displacements of a finite-length thin elastic rod in a viscous fluid driven by prescribed curvature, $\kappa_0(s, t)$, (equivalently, prescribed moments) along the body with free ends. The shape of the rod is determined by the balance between elastic forces and viscous drag. The vertical displacement, $y(s, t)$ satisfies

$$(4) \quad \zeta_{\perp} y_t = -B(y_{ss} - \kappa_0)_{ss},$$

$$(5) \quad y_{ss} - \kappa_0 = 0, (y_{ss} - \kappa_0)_s = 0, \text{ at } s = 0, L.$$

Here ζ_{\perp} is the perpendicular drag coefficient and B is the bending stiffness of the body.

Nondimensionalizing equation (4) using the body length L and the period of the driving force T results in the dimensionless parameter we call the body response time:

$$(6) \quad G = \frac{T}{B^{-1}\zeta_{\perp}L^4} = \frac{\text{period of motion}}{\text{elasto-hydrodynamic beam relaxation time}}.$$

We note that G^{-1} could be called a body relaxation time. The same nondimensional group has appeared previously, but has been interpreted differently. In [16] a quantity similar to G was considered an ‘‘effective viscosity’’ of growing elastic filaments. The Sperm number ($Sp = G^{-1/4}$) is the ratio of the body length to the viscous decay length [14]. This interpretation is natural when considering filaments driven at one end rather than along the body as we do here.

We change variables from displacement to curvature deviation $c(s, t) = \kappa(s, t) - \kappa_0(s, t)$ to facilitate comparing with large amplitude simulations. For small displacements $y_{ss}(s, t) \approx \kappa(s, t)$, and equation (4), (non-dimensionalized) becomes $c_t = -Gc_{ssss} - \frac{\partial \kappa_0}{\partial t}$, with boundary conditions, $c = 0, c_s = 0$ at $s = 0, L$. For a given κ_0 , we use an orthogonal function expansion to solve the non-dimensional equations for $c(s, t)$. Let the driving curvature be given as $\kappa_0(s, t) = \sum_{k=1}^{\infty} \alpha_k^{\infty} e^{2\pi i k t} \Psi_k(s)$, where μ_k and $\Psi_k(s)$ are the k^{th} eigenvalues and eigenfunctions, respectively. The expansion coefficients of the realized curvature, α_k , are then $\alpha_k = \alpha_k^{\infty} \left(1 - \left(1 - \frac{G\mu_k}{2\pi i} \right)^{-1} \right)$. From this solution we can see that as the rod is stiffened ($G \rightarrow \infty$), the resultant curvature tends to the prescribed curvature, $\alpha_k \rightarrow \alpha_k^{\infty}$. We also see that for softer rods, i.e. smaller values of the body response time G , the amplitude of the curvature decreases and there is a phase lag relative to the prescribed shape.

3.2. Linear theory: viscoelastic fluids. We can modify the linear theory for elastic rods to include fluid elasticity. This is similar to what was done in [17, 15]. As in equation (4) we can write a force balance relation between the force on a fluid and from the beam as

$$f_{\text{fluid}} - B(y_{ss} - \kappa_0)_{ss} = 0,$$

where the f_{fluid} represents the normal force on the rod from the viscoelastic fluid. If we define the fluid force to be based on the total deviatoric stress $\boldsymbol{\tau} = \dot{\boldsymbol{\gamma}} + \boldsymbol{\tau}_p$ then (upon linearization) using equation (3):

$$(7) \quad \text{De } \dot{f}_{\text{fluid}} + f_{\text{fluid}} = (1 + \xi)f_{\text{vis}} + \text{De } \dot{f}_{\text{vis}},$$

where f_{vis} is the viscous drag force. Note that given the form of the system in equations (2)-(3), we have assumed a total viscosity of $1 + \xi$. The swimmer motion is time-periodic so we take the Fourier transform in time of equation (7) to solve for viscoelastic modifications to the fluid drag. This yields, $\hat{f}_{\text{fluid}} = \left(\frac{1 + \xi + 2\pi i \text{De}}{1 + 2\pi i \text{De}} \right) \hat{f}_{\text{vis}}$.

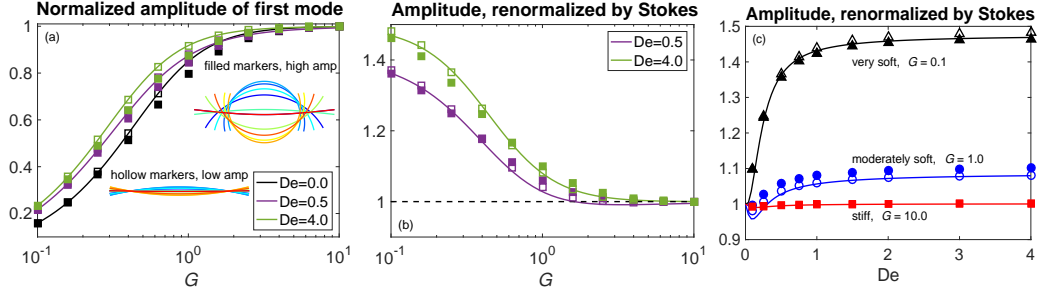


FIGURE 3. (a) Normalized amplitude, theoretical (lines) and simulations (markers). (b)-(c) Data renormalized by Stokes.

As in the viscous theory, we can solve for modifications to the curvature from body stiffness and use the modifications to the fluid drag to account for the fluid elasticity:

$$(8) \quad \alpha_k = \alpha_k^\infty \left(1 - \left(1 - \frac{G\mu_k}{\zeta_\perp 2\pi i} \right)^{-1} \right), \quad \text{with} \quad \zeta_\perp = \frac{1 + \xi + 2\pi i De}{1 + 2\pi i De}.$$

The coefficients in equation (8) give an analytical expression for the modifications to the rod shapes relative to the prescribed shapes as fluid and body elasticity are varied.

3.3. Elastic shape changes: theory and numerical comparison. In order to compare these predicted shape changes with our numerical simulations we prescribe a curvature of the form $\kappa_0(s, t) = A \sin(2\pi t)$. The prescribed standing wave of constant curvature corresponds to a motion through circular arcs with peak curvature A . By symmetry, this motion does not result in any horizontal translation of the body. We refer to these non-translating “swimmers” as *flexors*. We consider both low and high amplitude curvatures, $A = 0.5$ and $A = 4.0$. The shapes are shown inset in figure 3(a).

In figure 3 we plot the theoretical predictions from equation (8) (solid lines) along with values computed from numerical simulations; low amplitude ($A = 0.5$) are indicated by hollow markers, and high amplitude ($A = 4.0$) are indicated with filled markers. In figure 3(a) we plot the normalized amplitude of the first mode ($|\alpha_1|/|\alpha_1^\infty|$) to see how the amplitude deviates from the prescribed amplitude as a function of dimensionless stiffness (body response time). We see that generically the amplitude of the flexor decreases as the flexor is softened for fixed De . For sufficiently soft flexors ($G \lesssim 1$) viscoelasticity increases the amplitude monotonically with De , but for stiffer swimmers the amplitude changes nonmonotonically with fluid elasticity.

In figures 3(b) and (c) we renormalize the data by the amplitude in a viscous fluid to see the effects of viscoelasticity more clearly. Again we see that fluid elasticity can increase the amplitude significantly for a soft flexor, but that effect is lost as the flexor is stiffened. When we plot the amplitude as a function of De for the *very soft*, *moderately soft* and *stiff* cases we see again that three qualitatively different regimes emerge. For *very soft* flexors the amplitude is monotonically increased by elasticity, for *moderately soft* flexors the response is non-monotonic, and can decrease or increase the amplitude, and for *stiff*

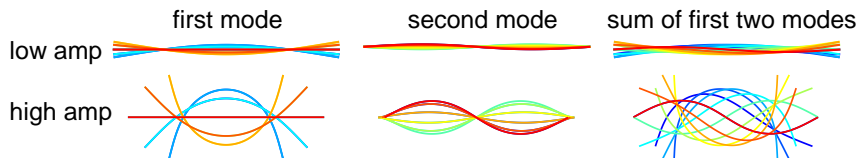


FIGURE 4. Shapes for first, second, and sum of first two modes for “two-mode” swimmer defined by equation (9). Snapshots of one period for low and high amplitude strokes.

flexors there is little change in the amplitude due to fluid elasticity. It is notable that the linear theory does such a good job predicting shape changes for low and high amplitude and for low and high Deborah number.

We note that we are showing results only for the first mode. For higher modes the trends are similar but the transition from stiff to soft behavior occurs at lower values of G because the eigenvalues μ_k increase with k .

4. ANALYSIS OF SWIMMING SPEED

In a viscous fluid, increasing the stroke amplitude will increase the swimming speed, and we can infer from section 3 that soft swimmers in a viscoelastic fluid sometimes obtain an amplitude boost over the corresponding swimmer in a Newtonian fluid. However when comparing swimmers in a viscoelastic fluid to those in a viscous fluid, even with an amplitude boost the viscoelastic swimmer may not swim faster than the viscous swimmer due to additional fluid elastic forces that the swimmer will encounter. Analytical expressions for infinite-length small amplitude swimmers show that a slow-down is generically expected for stiff swimmers in a viscoelastic fluid [1], but shape changes can lead to speed boosts [2]. It was conjectured [4] that speed boosts for finite-length swimmers were related to large tail stresses, and in [5] stroke asymmetries were correlated with both slow-downs and speed-ups. Here we will make a quantitative statement about the effect of elastic induced shape changes on swimming speed, isolating this effect from all other effects of fluid elasticity, and we will compare the analysis with numerical simulations.

4.1. Swimming speed: two-mode swimmer. To keep the analysis simple we define a gait whose swimming speed in a viscous fluid we can compute analytically. We define a “two-mode swimmer” given by the curvature:

$$(9) \quad \kappa(s, t) = \alpha_1 \cos(2\pi t/T + \phi_1) \Psi_1(s) + \alpha_2 \cos(2\pi t/T + \phi_2) \Psi_2(s),$$

where the $\Psi_i(s)$ for $i = 1, 2$, are the first and second bending modes. The modulation of a single mode results in a standing wave and will not translate in a Newtonian fluid. We use a sum of the first two modes with a phase difference to generate a nonreciprocal motion. Shapes of the first, second, and sum of the first and second modes are plotted in figure 4 for both low and high amplitudes.

Using resistive force theory one can derive the (time-averaged) swimming speed for a given, small amplitude, motion:

$$(10) \quad \langle U \rangle = \left(\frac{\zeta_{\perp}}{\zeta_{\parallel}} - 1 \right) \frac{1}{LT} \int_0^T \int_0^L y_s y_t ds dt,$$

where U is the swimming speed, $y(s, t)$ is the vertical displacement of the swimmer, and ζ_{\perp} and ζ_{\parallel} are the perpendicular and parallel drag coefficients, respectively, [13, 14]. For small amplitudes, the shape of the swimmer (up to translation and rotation) is given by integrating equation (9) twice in space to compute the swimming speed via equation (10). The swimming speed (in a viscous fluid) for the two-mode swimmer is proportional to the product of the amplitudes and the sine of the phase difference: $\langle U \rangle \propto \alpha_1 \alpha_2 \sin(\phi_2 - \phi_1)$. Using the expressions that give the phase and amplitude dependence on De and G in equation (8), we can then compute a swimming speed in a viscous fluid that depends on the shape changes. We will refer to this swimming speed as the stroke-induced swimming speed and plot this quantity (normalized by the viscous swimming speed) as a function of the so-called stroke-Deborah number, Stroke_{De} , a parameter that indexes the stroke changes as De is varied [5].

As with the flexor, we see in figure 5 (a) the emergence of three regimes. Shape changes boost swimming speed if the swimmer is *very soft*, a smaller boost is obtained for the *moderately soft* swimmer, and additionally there is a non-monotonic response to increasing elasticity including a regime where shape changes slow down the swimmer, and finally if the swimmer is *stiff* there is a negligible effect.

4.2. Swimming speed: theory and numerical comparison. We simulate a two-mode swimmer of both low and high amplitude by prescribing a curvature of the form equation (9) with $\alpha_1 = 0.8K_0$, $\alpha_2 = 0.6K_0$, $\phi_2 - \phi_1 = \pi/2$, for $K_0 = 0.5$ (low), and 4.0 (high). These values come from projections of the stroke used to generate figure 1. The Stokes-normalized swimming speeds for a *very soft*, *moderately soft*, and *stiff* swimmer at both low (hollow markers) and high (filled markers) amplitude are plotted in figure 5 (b). We note that the three regimes seen in figure 5 (a) still emerge from these simulations, but the simulation results always predict slower speeds over the stroke-induced swimming speeds. The ratio of swimming speed to stroke-induced swimming speed is shown in figure 5 (c). This quantity can be interpreted as the effect of fluid elasticity that is *not* related to shape changes. It is notable that these curves collapse onto a single curve for the low amplitude swimmers at all stiffnesses as well as the high-amplitude swimmer in the very soft regime. This additional elastic fluid effect on swimming speed is likely to be highly stroke dependent.

The additional effects of fluid elasticity are fundamentally different for the large amplitude, large De regime. In figure 5 (d) we plot the ratio of swimming speeds for the high-to-low amplitude strokes, and see that for $De > 1$ (for sufficiently stiff swimmers) a significant difference in swimming speed arises. This difference is not related to shape changes because, like the flexor, the elastic-induced shape changes predicted by the theory for the two-mode swimmer agree very well with the simulation results, for all De , at low and high amplitudes; see figure 6. At low amplitude (not shown) the relative error between

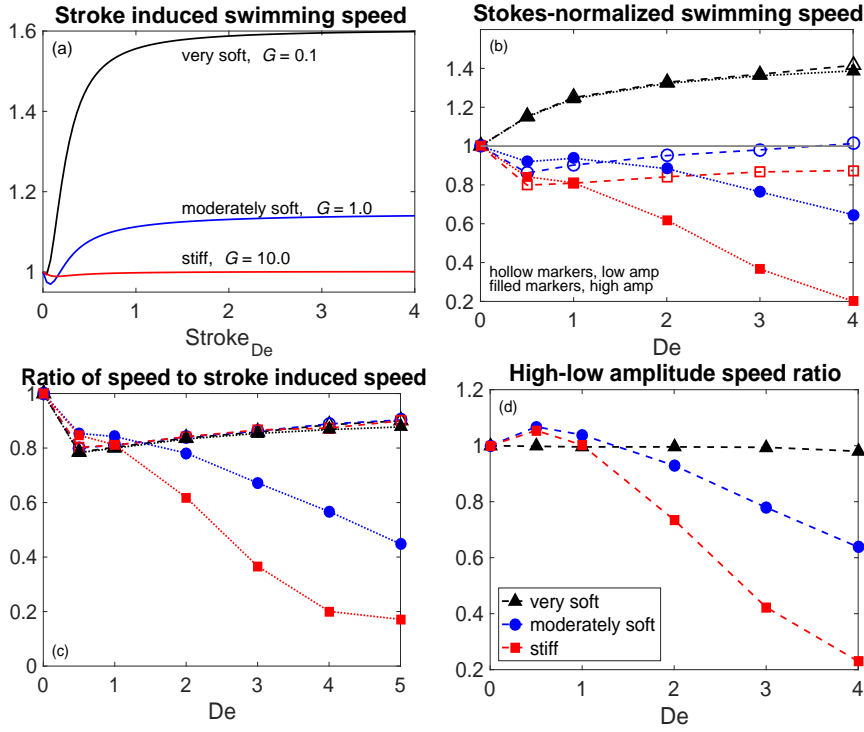


FIGURE 5. (a) Theoretically predicted stroke-induced swimming speed (normalized). (b) Stokes-normalized swimming speed in simulations with the two-mode swimmer. (c) Ratio of speed to stroke-induced speed for low and high amplitude strokes. (d) Ratio of high to low amplitude swimming speed. (Dashed lines are for graphical interpretation).

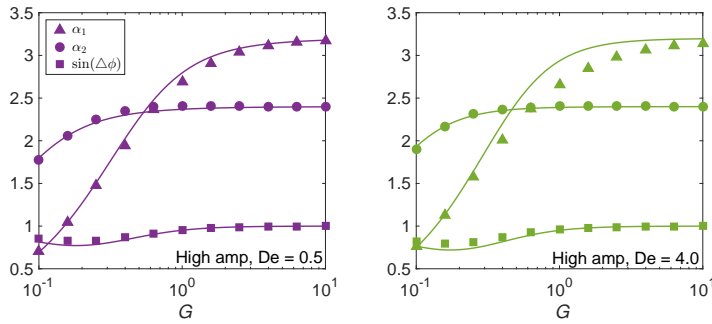


FIGURE 6. Theoretical predictions (solid lines) for two-mode swimmer shapes for varying G , low and high De . Markers show simulation results for high amplitude.

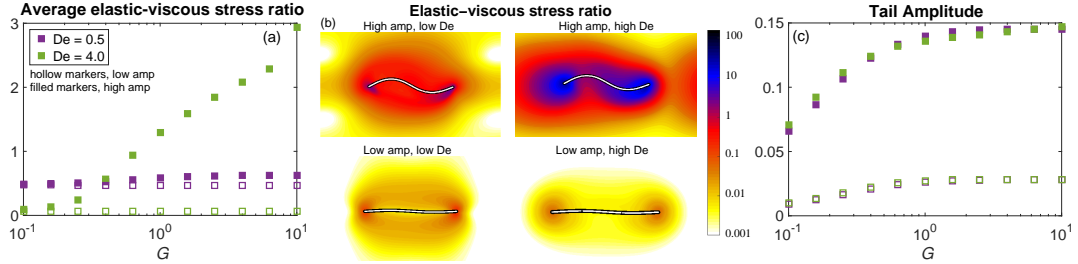


FIGURE 7. (a) Average elastic-viscous stress ratio in two-mode swimmer. (b) Elastic-viscous stress ratio for stiff swimmers. (c) Tail amplitudes.

theoretical and numerical predictions is less than 1%, and for high amplitude the error at low De is at most 5% and at high De the error is at most 9%. These results indicate that the theoretically predicted shape changes and their isolated effects on swimming speed can be well approximated by the analytical results for all De and all amplitudes. A mechanistic understanding is lacking to explain what causes the dramatic slow-downs of swimmers in the high amplitude, high De regime.

We conjecture that the slow-downs in the high amplitude, high De regime must be attributed in part to the large localized stresses that accumulate near the body [4, 5]. To explore this conjecture, in figure 7 (a) we plot the average elastic to viscous stress ratio over a range of body response time G for both low (hollow markers) and high amplitude (filled markers) strokes for $De = 0.5, 4.0$. There is a notable transition in the stress ratio in the high De , high amplitude swimmer as the body is stiffened, while this stress ratio is flat for both low amplitude and low De swimmers. *Stiff* swimmer shapes along with the elastic-viscous stress ratio are plotted on a log-scale in figure 7 (b). The low amplitude strokes are surrounded by elastic stresses that are at least two orders of magnitude smaller than the high amplitude strokes, but even at large amplitude the low De swimmer still has relatively low stress near the body. Lastly, we plot the tail amplitude, as one measure of the swimmer stroke, in figure 7 (c). We see that for sufficiently soft swimmers the “high amplitude” stroke has a lower amplitude, which explains why in figure 5 the *very soft* high amplitude swimmer behaves like the low amplitude swimmers. For the high amplitude strokes it is only in the large amplitude *and* large De regime where significant stress accumulates near the swimmer.

5. CONCLUSIONS

In [5] we showed that stroke related speed-ups depend on body stiffness, and the analysis from this paper shows explicitly how the stroke changes depend on body stiffness and fluid elasticity through two dimensionless “relaxation times”: the fluid relaxation time, De and the body relaxation time, G^{-1} . When we look at apparently contradictory results from the literature, we see that calculating G will determine into which regime the swimmer falls. In [6] the Sperm number is reported to be between 0.5 – 2.5, but even with the awareness that

these are soft swimmers the authors “conjecture that the effect [due to shape changes] is not significant”. We use their reported parameters¹ and a characteristic frequency of 1s^{-1} , and find $G \approx 0.43$, which is in the *very soft* regime where shape changes give significant speed-ups, agreeing with their results. In [7] the parameter reported for what they consider to be a soft swimmer is $B = 2$. However their swimmer length is $L = 0.6$ mm (with characteristic length 1 mm) hence an equivalent dimensionless body response time G must be multiplied by $L^{-4} \approx 7.7$. This pushes their “soft” simulations into the *stiff* regime where there are no speed-ups from shape changes, also agreeing with their results. Furthermore, in [7] it is conjectured that stress diffusion, used to regularize the simulations in [4, 5], is the source of the speed-ups, but the speed-ups we see are theoretically predicted, and realized in our simulations, even in the low amplitude regime where no regularization is necessary.

In our analysis we quantify the effect of body and fluid elastic-induced shape changes on swimming speed. We see that the shape change analysis holds for all amplitudes and all De , and we see an additional elastic slow-down that is reminiscent of the type of slow-down predicted by asymptotic analysis of infinite-length swimmers. It may be tractable to apply asymptotic analysis [2, 18] to determine the form of the elastic slow-down for low amplitude finite-length swimmers. A fundamentally different regime arises for large amplitude swimmers in highly elastic fluids. A different approach is needed to understand the mechanisms that cause large localized stresses and their effect on swimming.

The authors would like to thank Henry Fu and Roberto Zenit for interesting discussions and suggestions on this work, and Michael Shelley for suggesting the term “flexors”. The work of RDG was partially supported by NSF grants DMS-1160438 and DMS-1226386.

6. APPENDIX

The analysis in this paper made use of resistive force theory which relates the drag force and velocity on a long thin cylindrical object. Our numerical simulations are in two spatial dimensions, and standard resistive force theory does not apply. We estimate an effective 2D drag coefficient (to use in equation (6)) numerically by examining the eigenvalues of the discrete operators linearized about a flat configuration, $(x, y) = (s, 0)$. The vertical displacement of the points satisfies the differential equation $\dot{\mathbf{y}} = M\mathbf{A}\mathbf{y}$, where A is the operator corresponding to the linearization of the bending force operator, and M is the discrete mobility matrix which maps forces on points to vertical velocities.

We compute an effective drag coefficient for each eigenvector, $\zeta_k = \lambda_k^A / \lambda_k^{MA}$, where λ_k^A is the k^{th} eigenvalue of A and λ_k^{MA} is the k^{th} eigenvalue of MA . Note that in resistive force theory, the mobility matrix is approximated as a scalar, and the above definition reduces to the usual drag coefficient. We use the method of regularized Stokelets [19] for the mobility matrix, and with $N_s = 501$ points on the swimmer the eigenvalues of A are within 1% of the eigenvalues of the continuous operator. For the first four nontrivial modes,

¹ $L = 25\text{mm}$, cross-sectional radius $a = 62.5\mu\text{m}$, Young’s modulus $E = 80$ GPa, viscosity $\mu = 2.7$ Pa-s. For moment of inertia $I = \pi a^4/4$, we get $B = EI = 9.6 \times 10^{-7}$, $\zeta = 4\pi\mu/\ln(L/a)$, and thus $G = \frac{BT}{\zeta L^4} = \frac{9.6 \times 10^{-7} \ln(400)}{4\pi \cdot 2.7 (25 \times 10^{-3})^4} \approx 0.43$.

$k = 1 - 4$, the corresponding eigenvalues are $\lambda_k^A = \{-4.97e+02, -3.77e+03, -1.45e+04, -3.96e+04\}$, $\lambda_k^{MA} = \{-1.53e+01, -8.79e+01, -2.65e+02, -5.93e+02\}$ and the resulting drag coefficients are $\zeta_k = \{32.55, 42.94, 54.69, 66.84\}$.

REFERENCES

- [1] Eric Lauga. Propulsion in a viscoelastic fluid. *Phys. Fluids*, 19(8):83104, 2007.
- [2] Emily E Riley and Eric Lauga. Enhanced active swimming in viscoelastic fluids. *EPL (Europhysics Letters)*, 108(3):34003, 2014.
- [3] X N Shen and Paulo E Arratia. Undulatory swimming in viscoelastic fluids. *Physical review letters*, 106(20):208101, 2011.
- [4] Joseph Teran, Lisa Fauci, and Michael Shelley. Viscoelastic fluid response can increase the speed and efficiency of a free swimmer. *Physical review letters*, 104(3):38101, January 2010.
- [5] Becca Thomases and Robert D. Guy. Mechanisms of Elastic Enhancement and Hindrance for Finite-Length Undulatory Swimmers in Viscoelastic Fluids. *Physical Review Letters*, 113(9):098102, August 2014.
- [6] Julian Espinosa-Garcia, Eric Lauga, Roberto Zenit, San Diego, and La Jolla. Fluid elasticity increases the locomotion of flexible swimmers. *Phys. Fluids*, 25(3):31701, 2013.
- [7] Daniel Salazar, Alexandre M Roma, and Hector D Cenicerros. Numerical study of an inextensible, finite swimmer in stokesian viscoelastic flow. *Phys. Fluids*, 28(6):063101, 2016.
- [8] Robert D Guy and Becca Thomases. Computational challenges for simulating strongly elastic flows in biology. In *Complex Fluids in Biological Systems*, pages 359–397. Springer, 2015.
- [9] Lisa J Fauci and Charles S Peskin. A computational model of aquatic animal locomotion. *Journal of Computational Physics*, 77(1):85–108, 1988.
- [10] R. B. Bird, O. Hassager, R. C. Armstrong, and C. F. Curtiss. *Dynamics of Polymeric Liquids, Vol. 2: Kinetic Theory*. John Wiley and Sons, 1980.
- [11] R Sureshkumar and Antony N Beris. Effect of artificial stress diffusivity on the stability of numerical calculations and the flow dynamics of time-dependent viscoelastic flows. *J. Non-Newton. Fluid Mech.*, 60(1):53–80, 1995.
- [12] Becca Thomases. An analysis of the effect of stress diffusion on the dynamics of creeping viscoelastic flow. *Journal of Non-Newtonian Fluid Mechanics*, 166(21-22):1221–1228, 2011.
- [13] Chris H Wiggins and Raymond E Goldstein. Flexive and propulsive dynamics of elastica at low reynolds number. *Physical Review Letters*, 80(17):3879, 1998.
- [14] Eric Lauga and Thomas R Powers. The hydrodynamics of swimming microorganisms. *Reports on Progress in Physics*, 72(9):096601, 2009.
- [15] Henry C Fu, Charles W Wolgemuth, and Thomas R Powers. Beating patterns of filaments in viscoelastic fluids. *Physical Review E*, 78(4):041913, 2008.
- [16] Michael J Shelley and Tetsuji Ueda. The stokesian hydrodynamics of flexing, stretching filaments. *Physica D: Nonlinear Phenomena*, 146(1):221–245, 2000.
- [17] Glenn R Fulford, David F Katz, and Robert L Powell. Swimming of spermatozoa in a linear viscoelastic fluid. *Biorheology*, 35(4):295–309, 1998.
- [18] Gwynn J Elfring and Gaurav Goyal. The effect of gait on swimming in viscoelastic fluids. *Journal of Non-Newtonian Fluid Mechanics*, 234:8–14, 2016.
- [19] Ricardo Cortez. The method of regularized stokeslets. *SIAM Journal on Scientific Computing*, 23(4):1204–1225, 2001.